This is to certify that the

thesis entitled

A COMPACT NON-QUASI-STATIC MOSFET DEVICE MODEL

presented by

Chi-Jung Huang

has been accepted towards fulfillment
of the requirements for

Master's degree in Electrical
Engineering

Timothy Grotjan
Major professor

Date 11-9-88

A COMPACT NON-QUASI-STATIC MOSFET DEVICE MODEL

By

Chi-Jung Huang

A THESIS

Submitted to
Michigan State University
in partial fulfillment of the requirements
for the degree of

MASTER OF SCIENCE

Department of Electrical Energineering and System Sciece

1988

ABSTRACT

A COMPACT NON-QUASI-STATIC MOSFET DEVICE MODEL

By

Chi-Jung Huang

Circuit simulators whose MOSFET device models adopt the quasi-static assumption assume that the channel charge distribution can be built up instantaneously. Such quasi-static device models are becoming inadequate as the trend of increasing the speed of MOS integrated circuits operation continues. The purpose of this thesis is to investigate the significance of the non-quasi-static (NQS) behavior of the MOSFET under various circuit application. A compact device model was developed by approximating the channel charge distribution. This device model was then implemented into a circuit simulator which was used in various circuit applications to investigate the importance of the NQS effect. This work shows that for circuits with small capacitive loading or for the circuits operating in the near-threshold or subthreshold regions, the QS assumption is inadequate for the accurate determination of the circuit timing.

ACKNOWLEDGMENTS

I would like to express my appreciation to my academic advisor Dr. Timothy A. Grotjohn for his guidance and for his many valuable suggestions while reviewing my manuscript. I am also very grateful to my wife Su-Yun for her patience and encourgements.

TABLE OF CONTENTS

LIST OF TABLES

LIST OF FIGURES

CHAPTER 1

Introduction

1.1 Review of MOSFET Models

MOSFET device models are used in circuit simulators to represent the device characteristics in the form of analytical mathematical equations for the regions of operation. As shown in Fig. 1, a MOSFET has four regions of operations:

1) Linear region:

Both the drain and source ends of the channel are turned on. The mathematical criterion for a n-channel MOSFET in the linear region is: $V_{gs} > V_{th}$ and $0 < V_{ds} < V_{dsat}$, where V_{th} is the threshold voltage for Vgs to turn on the source end and V_{dsat} is the voltage for V_{ds} to pinch-off the drain end.

2) Saturation region:

The drain end is pinched-off, but the source end is turned on. The criterion is: $V_{gs} > V_{th}$ and $V_{ds} > V_{dsat}$.

3) Subthreshold / Depletion region:

The drain end is pinched-off and the source end is slightly turned on. The criterion is: $V_{fb} + V_{bs} < V_{gs} < V_{th}$, where V_{fb} is the flat band voltage for the MOSFET.

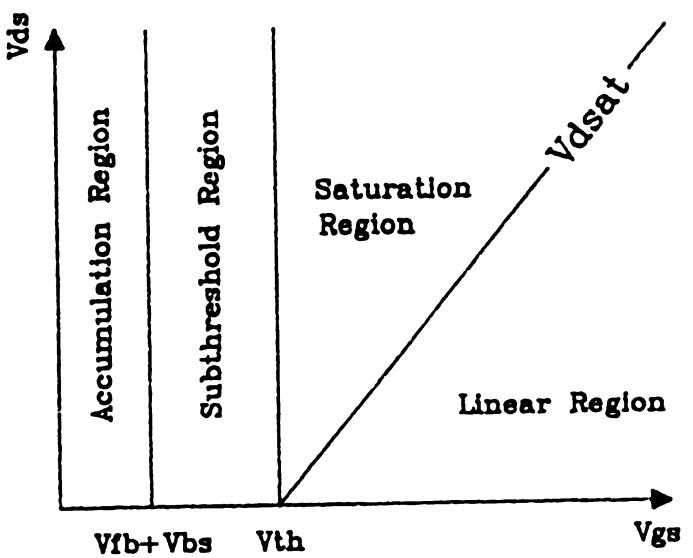

Fig. 1. The four regions of operation of a N-channel MOSFET.

4) Accumulation region:

In this region, both the drain and source are pinched-off. The majority carriers dominant in the channel and the channel is non-conducting. The criterion is : $V_{gs} < V_{fb} + V_{bs}$.

Depending on their applications, these device models may be further distinguished into the DC, AC, or transient type simulation:

1) DC:

A DC simulation solves for the circuit parameters, typically the DC voltages on the nodes and the DC currents through the branches of the circuit, under constant power supplies and constant input voltages. In general, nodal analysis is performed to converge the initial guess of the circuit parameters to a final solution.

2) AC:

An AC simulation solves the steady state currents and voltages when small signals are added to DC biases. A linearized model around the DC bias is used for the nodal analysis.

3) Transient:

A transient type simulation solves for the circuit behavior by applying large signals to the input nodes. A transient simulator

solves the dynamical behavior of the circuit.

The sophistication and complexity of currently used DC, AC and transient models vary widely depending on the accuracy and operation range required.

Most of the currently used circuit simulators, such as Spice [1], represent the MOSFET with a lumped equivalent circuit model as seen in Fig. 2a. The lumped models adopt the Quasi-Static (QS) assumption that the charges in the channel can change immediately when the voltages on the four terminals of the MOSFET are changed. However, since channel charges can only be varied by the current flowing from the drain or the source, the QS assumption is not valid for fast turn-on or turn-off signals applied to the terminals of MOSFET's. For fast signals, a distributed device model as shown in Fig. 2b should be considered. When MOS integrated circuits are operated with fast signals, the distributed or Non-Quasi-Static (NQS) effects become significant. Thus, circuit simulators using quasi-static MOSFET models need careful evaluations in the regions where the quasi-static assumption may not be valid.

Recently, several attempts have been made to include the non-quasi-static behavior into the device model for the MOSFET. Two methods have been published which include NQS behavior in large signal transient simu-

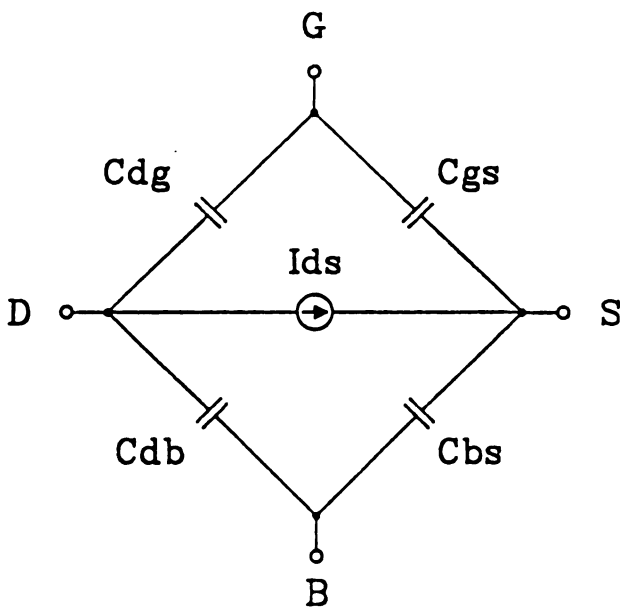

(a)

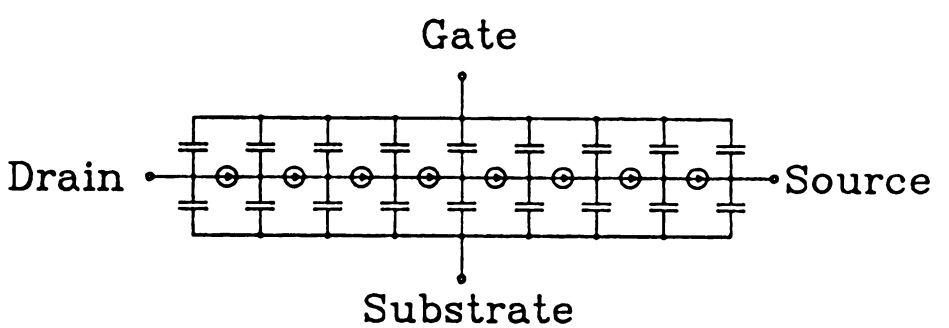

(b)

Fig. 2. MOSFET device model of: (a) lumped equivalent device model; (b) distributed device model.

lation.

The first one, proposed by Mancini, Turchetti and Masetti [2], solves the transient continuity equation along the channel of MOSFET. It is observed that the numerical solution of the continuity equation describes the NQS channel charges. Unfortunately, this approach is limited to small circuits due to the long computational time needed for solving the differential equation.

The second one, also by Turchetti, Mancini and Masetti [3], solves an approximating ordinary differential equation for NQS channel charges under strong inversion conditions. This CAD model, although efficient, is inadequate for the near-threshold and subthreshold region where NQS behavior is significant due to the slow diffusion mechanism which is dominant in the weak inversion condition.

1.2 Statement of Purpose

The major purpose of this work is to efficiently include the subthreshold current in an NQS model and to make the necessary improvements or modifications to the model so that all regions are accurately simulated. By implementing this compact NQS MOSFET model into a circuit simulator, the significance of the NQS behavior for the MOSFET in each region of operation can be evaluated. Additionally, the importance of the NQS effect

in MOSFET device models can be investigated in various circuit applications.

1.3 Thesis Preview

In chapter two, the equations of this compact NQS MOSFET device model are developed. By appropriately solving the continuity equation, the numerical model of Turchetti's work [2] is formulated in Section 2.2. The weighted residue method is then applied to the numerical model to obtain an ordinary differential equation which can be efficiently implemented into a form for computer solution (Section 2.3). The method of calculating the carrier concentrations at each end of the channel is described in Section 2.4. Some further improvements made by comparing to an exact numerical solution are then explained in Section 2.6.

The formulation of the NQS circuit simulator is described in chapter three. First, the expressions for the charges on the four terminals of the MOSFET are derived in Section 3.1. The implementation of the terminal charges along with other device parameters into the TABLET (Table model based Transient simulator) program [4] is detailed in Section 3.2.

Various applications using this simulator are investigated in chapter four. Comparision between NQS simulations, QS simulations and measurements are made to verify the results of the simulations.

The significance of NQS effects on the MOSFET device models is concluded in chapter five.

CHAPTER 2

Formulation of the NQS Model

In this chapter, the formulation of the compact NQS model is presented. Since the quasi-static behavior of an intrinsic, long channel NMOS device has been thoroughly studied [6], the NQS model is developed using similiar assumptions as the quasi-static model. Important assumptions inlude the gradual channel approximation and depletion approximation. Formulation of the NQS model in this way will permit comparision of the QS and NQS device models.

Brews's charge sheet model [7] which compresses the inversion layer of minority carriers into a conducting plane of zero thickness has been well verified in most applications. The NQS model adopts such a charge-sheet formulation since it leads to simple algebraic equations.

The basic equations of the MOSFET device are reviewed in Section 2.1. Section 2.2 develops the NQS numerical model which solves for the channel charge behavior in terms of a partial differential equation. In Section 2.3, the compact NQS model which approximates the channel charge distribution is formulated. Section 2.4 describes an efficient procedure of solving the boundary conditions for the compact model. Non-quasi-static drain current and source current expressions are derived in Section 2.5.

The last section presents further improvements which are made to the currents.

2.1 Basic Equations of MOSFET

The geometry of a N-channel MOSFET is shown in Fig. 3. Due to the attraction force of the gate voltage, the minority carriers (electrons) form an inversion layer at the oxide-semiconductor interface. Electrons, which flow in the channel due to the drift or diffusion mechanism, contribute to the conduction current. The x axis is penetrating into the semiconductor, the y axis is parallel to the flow of the electrons, and the z axis is transverse to the electron flow. The width and length of the channel are given by Z and L respectively.

The NQS model solves for the current and the charge density at each point in the channel with respect to time. The three primary equations formulated to describe the NQS behavior of the MOSFET are:

1) The continuity equation which relates the NQS charge and the NQS current.
2) The current transport equation which relates the current with the potential and the charge density.
3) The charge neutrality equation which relates the mobile charge density with the bulk and gate charge density.

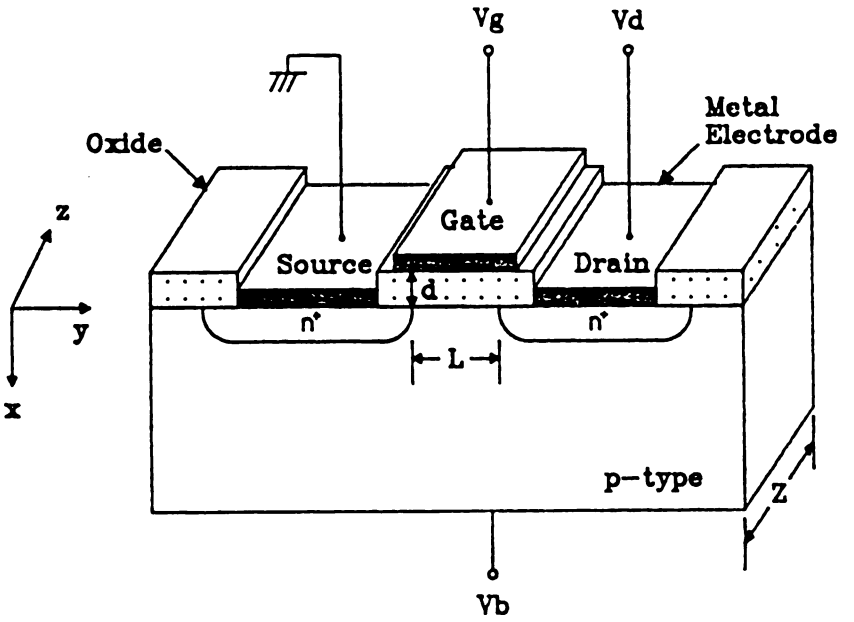

Fig. 3. Schematic digram of a N-channel MOSFET.

These equations are derived in the following sections.

2.1.1 Continuity Equation

For the case of the one dimensional current flow, the continuity equation may be expressed as

$$\frac{\partial n(x,y,t)}{\partial t} = \frac{1}{q}\frac{\partial J(x,y,t)}{\partial y}$$

assuming that the recombination and generation are negligible. By integrating over the current flow cross section, i.e.

$$\int_0^Z \int_0^{x_i} \frac{\partial n}{\partial t} dx dz = \int_0^Z \int_0^{x_i} \frac{1}{q}\frac{\partial J}{\partial y} dx dz$$

one obtains,

$$Z \frac{\partial}{\partial t} \int_0^{x_i} qn(x,y,t)dx = \frac{\partial}{\partial y} I(y,t) \qquad (2.1a)$$

where x_i is the intrinsic point where the minority carrier density is negligible. $I(y,t)$ is the current flowing through the cross section at point y of the channel. Additionally, $Q_n(y,t)$ is defined as the charge density per unit area at point y of the channel for time t, i.e.

$$Q_n(y,t) = \int_0^{x_i} -qn(x,y,t)dx. \qquad (2.1b)$$

Combining (2.1a) and (2.1b), one may reformulate the continuity equation as

$$-Z\frac{\partial}{\partial t} Q_n(y,t) = \frac{\partial}{\partial y} I(y,t). \qquad (2.2)$$

Equation (2.2) is the continuity equation relating the charge density $Q_n(y,t)$ and the current $I(y,t)$ at point y and time t.

2.1.2 Current Transport Equation

Consider both the drift and diffusion currents, the electron current density at the (x,y) position for a time t can be expressed as:

$$J_n(x,y,t) = q\mu_n n(x,y,t)E_y(y,t) + qD_n\frac{dn(x,y,t)}{dy} \tag{2.3}$$

where $n(x,y,t)$ is the electron concentration per unit volume, μ_n is the mobility of the electrons which is assumed to be constant, and E_y is the electric field in the y direction. Since the charge-sheet formulation compresses the electron layer into a surface charge, E_y can be written as

$$E_y(y,t) = -\frac{\partial\phi_s(y,t)}{\partial y}$$

where ϕ_s is the potential at the oxide-semiconductor interface. Also, by the Einstein relationship

$$D_n = \frac{kT}{q}\mu_n$$

where k represents the Boltzmann's constant, equation (2.3) can be written as

$$J_n(x,y,t) = -q\mu_n n(x,y,t)\frac{\partial\phi_s(y,t)}{\partial y} + \frac{q\mu_n}{\beta}\frac{\partial n(x,y,t)}{\partial y} \tag{2.4}$$

where $\beta = \frac{q}{kT}$.

The total device current flowing through the active cross section at each point of the channel can be obtained by integrating the current density over the cross section of current flow, i.e.

$$I(y,t) = \int_0^Z \int_0^{x_i} J_n(x,y)dxdz. \tag{2.5}$$

Substituting (2.4) into (2.5), one obtains

$$I(y,t) = Z\mu_n \left[\int_0^{x_i} -qn(x,y,t)\frac{\partial \phi_s(y,t)}{\partial y}dx + \frac{1}{\beta}\frac{\partial}{\partial y}\int_0^{x_i} qn(x,y,t)dx \right].$$

By (2.1b), it follows that

$$I(y,t) = Z\mu_n \left[Q_n(y,t)\frac{\partial \phi_s(y,t)}{\partial y} - \frac{1}{\beta}\frac{\partial Q_n(y,t)}{\partial y} \right]. \tag{2.6}$$

Equation (2.6) lays the foundation of the NQS model, since the current at point y of the channel at time t can now be expressed as an explicit function of surface potential and charge density. From (2.6), the drift current and diffusion current can be identified as the first and second term [8].

2.1.3 Charge Neutrality Equation

Fig. 4a and Fig. 4b show the energy band diagram and the space charges of the charge-sheet formulation at an arbitrary point y of the channel. When the inversion layer is turned-on by the gate bias and a non-zero drain bias is present for an enhancement mode MOSFET, the quasi-fermi

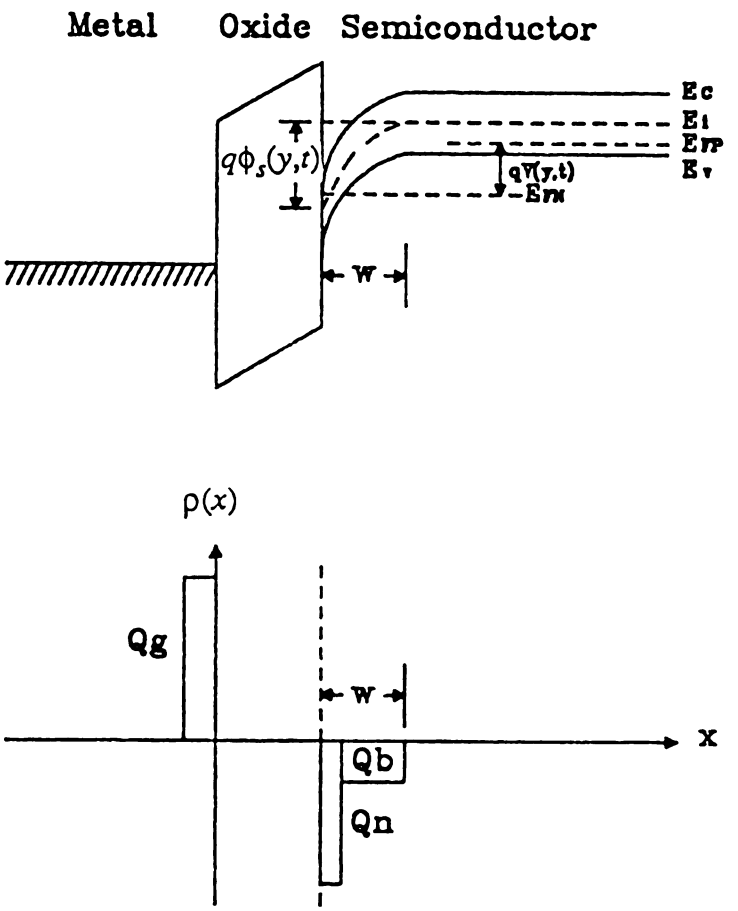

Fig. 4. At point y of the channel when the MOSFET is turned-on. (a) Energy band diagram. (b) Space charge density.

electron potential E_{FN} and the quasi-fermi hole potential E_{FP} splits. The splitting of the electron and hole quasi-fermi potential is given by $E_{FP} - E_{FN} = qV(y,t)$. $\phi_s(y,t)$ can then be expressed as:

$$\phi_s(y,t) = V(y,t) + 2\phi_B \ .$$

The voltage across the oxide is $V_G - V_{FB} - \phi_s$, and the charge density per unit area on the gate is

$$Q_g(y,t) = C_{ox} \left(V_G(t) - V_{FB} - \phi_s(y,t) \right) \qquad (2.7)$$

where C_{ox} is the oxide capacitance per unit area and V_{FB} is the flat band voltage for this device. Charge density per unit area for the bulk charge can be found by assuming that no majority carriers are present in the depletion region, i.e.

$$Q_b(y,t) = - qN_A W$$

where N_A is the doping of the substrate and W is the width of the depletion region. By solving Poisson's equation for the bulk charge region, one may find the expression for W to be

$$W = \sqrt{\frac{2\varepsilon_s}{qN_A} \left[\phi_s - V_B \right]}$$

where ε_s is the dielectric constant of the semiconductor. Therefore, the bulk charge density can be expressed as

$$Q_b(y,t) = - \sqrt{2\varepsilon_s qN_A \, (\phi_s(y,t) - V_B(t))}.$$

A more exact solution is [9]

$$Q_b(y,t) = -\sqrt{2\varepsilon_s q N_A(\,\phi_s(y,t) - V_B(t) - 1/\beta\,)}. \tag{2.8}$$

The charge neutrality equation in the charge-sheet model requires that

$$Q_n(y,t) = -\,Q_g(y,t) - Q_b(y,t)$$

or, from (2.7), (2.8)

$$Q_n(y,t) = -\,C_{ox}(\,V_G(t) - V_{FB} - \phi_s(y,t)\,) + C_{ox}\,\lambda\sqrt{\phi_s(y,t) - V_B(t) - 1/\beta} \tag{2.9}$$

where $\lambda = \dfrac{\sqrt{2\varepsilon_s q N_A}}{C_{ox}}$.

2.2 Formulation of the NQS Numerical Model

For simplicity, all physical quantities are normalized according to the Table 2.1 [2]. The three basic equations derived in Section 2.1 are reformulated as:

Normalized Continuity Equation:

$$\frac{\partial}{\partial t}Q_n(y,t) = \frac{\mu_n}{L^2}\frac{\partial}{\partial y}I(y,t) \tag{2.2n}$$

Normalized Current Transport Equation:

$$I(y,t) = -\,Q_n(y,t)\frac{\partial\phi_s(y,t)}{\partial y} + \frac{1}{\beta}\frac{\partial Q_n(y,t)}{\partial y} \tag{2.6n}$$

Normalized Charge Neutrality Equation:

$$Q_n(y,t) = V_G(t) - V_{FB} - \phi_s(y,t) - \lambda\sqrt{\phi_s(y,t) - V_B(t) - 1/\beta} \tag{2.9n}$$

By taking the spatial derivative with respect to y on both sides of the

Physical quantities	Normalized factors
$Q_n(y,t)$	$- C_{ox}$
y	L
$I(y,t)$	$\mu_n Z C_{ox} / L$

Table 2.1 Normalization factors.

charge neutrality equation (2.9n) and rearranging the terms, one obtains,

$$\frac{\partial \phi_s(y,t)}{\partial y} = -\left[1 + \frac{\lambda}{2\sqrt{\phi_s(y,t) - V_B(t) - 1/\beta}}\right]^{-1} \frac{\partial Q_n(y,t)}{\partial y}.$$

By substituting this expression into the current transport equation (2.6n), the non-quasi-static current along the channel can be written as

$$I(y,t) = \left[\frac{Q_n(y,t)}{1+\frac{\lambda}{2\sqrt{\phi_s(y,t) - V_B(t) - 1/\beta}}} + \frac{1}{\beta}\right] \frac{\partial Q_n(y,t)}{\partial y}. \qquad (2.10)$$

Equation (2.10) can be combined with continuity equation (2.2n) to obtain a partial differential equation which describes the non-quasi-static charge density $Q_n(y,t)$ as

$$\frac{\partial}{\partial y}\left[\left[\frac{Q_n(y,t)}{1+\frac{\lambda}{2\sqrt{\phi_s(y,t) - V_B(t) - 1/\beta}}} + \frac{1}{\beta}\right] \frac{\partial Q_n(y,t)}{\partial y}\right] = \frac{L^2}{\mu_n}\frac{\partial}{\partial t} Q_n(y,t). \qquad (2.11)$$

Also, by solving equation (2.9n), $\phi_s(y,t)$ can be expressed as

$$\phi_s(y,t) = V_G(t) - V_{FB} - Q_n(y,t) + \frac{\lambda^2}{2} - \lambda\left[\left(\frac{\lambda}{2}\right)^2 + V_G(t) - V_{FB} - Q_n(y,t) - V_B(t) - \frac{1}{\beta}\right]^{\frac{1}{2}} \qquad (2.12)$$

Equations (2.11) and (2.12) constitute the equations from which $Q_n(y,t)$ can be solved numerically provided that appropriate initial and

boundary conditions are given. In fact, conventional knowledge of deriving the quasi-static charge density is sufficient to solve for these conditions [1]. They are:

(a) Initial condition:

The dc drain current I_{DC} can be found in any conventional dc charge-sheet model. $\phi_s(y,0)$ can then be solved using the following implicit expression:

$$I_{DC} \cdot y = P(y,0) - P(0,0) \tag{2.13a}$$

where $P(\eta,0)$ can be expressed as the following

$$\begin{aligned} P(\eta,0) = &\left[V_G(0) - V_{FB} + \frac{1}{\beta}\right]\phi_s(\eta,0) - \frac{1}{2}\phi_s^2(\eta,0) \\ &- \frac{2}{3}\lambda\left[\phi_s(\eta,0) - V_B(0) - \frac{1}{\beta}\right]^{\frac{3}{2}} \\ &+ \frac{\lambda}{\beta}\left[\phi_s(\eta,0) - V_B(0) - \frac{1}{\beta}\right]^{\frac{1}{2}}. \end{aligned} \tag{2.13b}$$

Solving (2.13a), (2.13b) requires an iterative procedure. By substituting $\phi_s(y,0)$ into equation (2.9n), the initial charge density distribution $Q_n(y,0)$ can be solved.

(b) Boundary condition:

By using a QS model [1,6], $\phi_s(0,t)$ and $\phi_s(1,t)$ are found by solving the following implicit equation

$$\frac{\lambda^2}{\beta}\left\{\beta\left[\phi_s(y,t) - 2\phi_F - V(y)\right]\right\}$$
$$= \left[V_G(t) - V_{FB} - \phi_s(y,t)\right]^2 - \lambda^2\left[\phi_s(y,t) - V_B(t) - \frac{1}{\beta}\right] \qquad (2.14)$$

with $V(0) = V_S$ and $V(1) = V_D$ for $\phi_s(0,t)$ and $\phi_s(1,t)$ respectively. By iteratively solving (2.14), one obtains $\phi_s(0,t)$ and $\phi_s(1,t)$ which allows the boundary charge densities $Q_n(0,t)$ and $Q_n(1,t)$ to be determined.

2.3 Formulation of the Compact Model

In this section, an approximation is made for the behavior of the non-quasi-static charge distribution. Consider equation (2.11), one can make the approximation that

$$1 + \frac{\lambda}{2\sqrt{\phi_s(y,t) - V_B(t) - 1/\beta}} \approx \delta. \qquad (2.15)$$

Parameter δ takes into account the body factor and short channel effect [10]. This simplification is commonly used in strong inversion dc models since it improves the efficiency of the models [11,12]. In a transient analysis, though δ varies with time, one can still make the approximation that

$$\frac{Q_n(y,t)}{1+\frac{\lambda}{2\sqrt{\phi_s(y,t)-V_B(t)-1/\beta}}}+\frac{1}{\beta}\approx\frac{Q_n(y,t)}{\delta}+\frac{1}{\beta}. \qquad (2.16)$$

The justification is based on the following reasoning:

1) In the strong inversion region: typically in the strong inversion region, δ is in the range from 1 to 2. The approximation is reasonable.

2) In the weak inversion region: since Q_n is quite small,

$$\frac{Q_n(y,t)}{\delta} \ll \frac{1}{\beta}.$$

Thus, the accuracy of δ is of little importance and (2.16) is justified.

Using (2.16), (2.11) can be simplified to be

$$\frac{\partial}{\partial y}\left[\left[\frac{Q_n(y,t)}{\delta}+\frac{1}{\beta}\right]\frac{\partial Q_n(y,t)}{\partial y}\right] = \frac{L^2}{\mu_n}\frac{\partial}{\partial t}Q_n(y,t). \qquad (2.17)$$

One efficient method of obtaining an approximate solution is the weighted residual method which extracts an ordinary differential equation from equation (2.17) [3].

The use of the weighted residual method requires that an approximate expression be assumed for $Q_n(y,t)$. To formulate the approximate expression, consider a MOSFET operating in the linear region with a time varying signal being applied to the gate as in Fig. 5a. The non-quasi-static charge distribution for a rising and falling signal can be analyzed by the

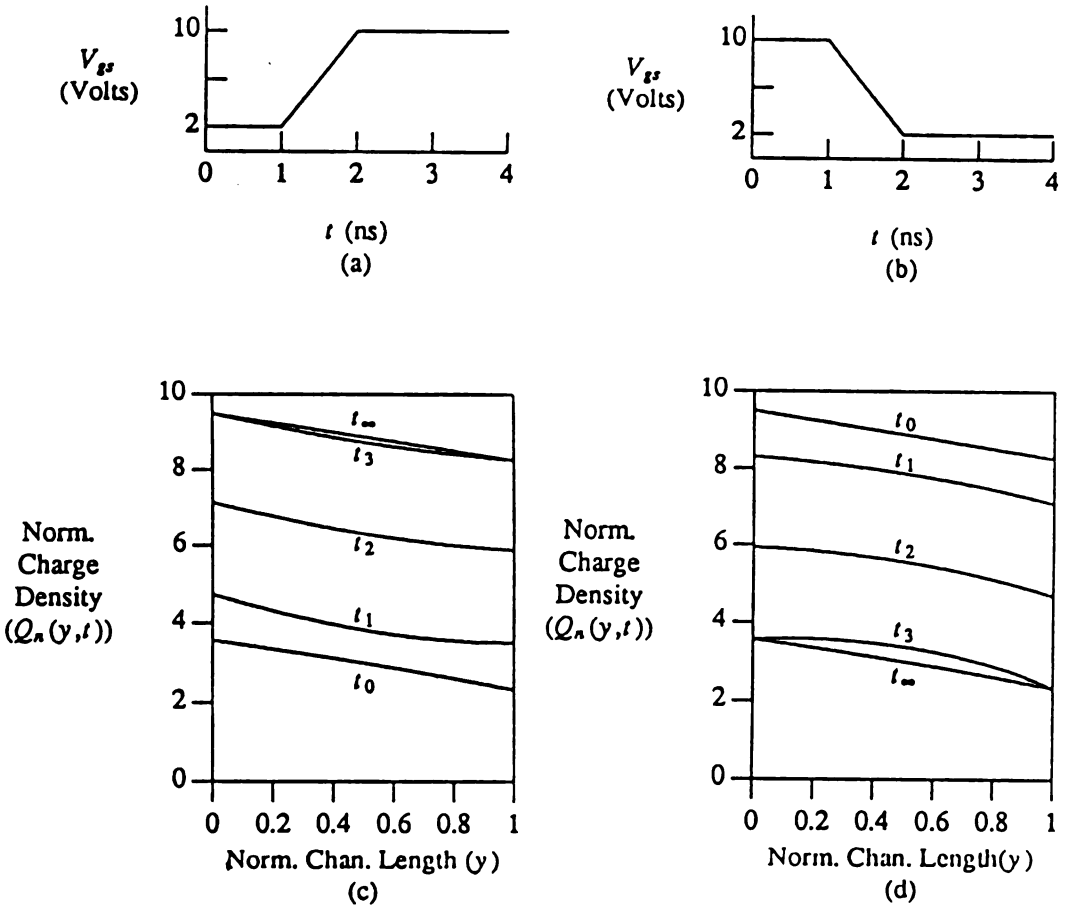

Fig. 5. Normalized time varying charge densities for a MOSFET with V_{FB} = - 0.8 volt, width = 10 μm, oxide thickness = 0.1 μm and doping = 10^{15} cm^{-3}. (a) The rising voltage ramp. (b) The falling voltage ramp. (c) Normalized charge density distributions when the voltage ramp of (a) is applied. t_0 = 0.9 ns, t_1 = 1.2 ns, t_2 = 1.6 ns, t_3 = 2.0 ns, V_D = 1.0 volt. (d) Normalized charge density distributions when the voltage ramp of (b) is applied. Time instants and V_D are the same as (c).

exact numerical model described in Section 2.2 and a typical result is shown in Fig. 5b and Fig. 5c.

It is reasonable that the first order accuracy can be maintained if one were to approximate the non-quasi-static charge distribution by a quadratic function, i.e.

$$\overline{Q}_n(y,t) = \alpha(t)y + \beta(t)(1-y) + B(t)(y^2-y) \tag{2.18}$$

where $B(t)$ is an undetermined function, and

$$\beta(t) = Q_n(0,t)$$
$$\alpha(t) = Q_n(1,t)$$

represent the boundary conditions.

The error, or residual, introduced by using the approximation can thus be defined as:

$$R = \frac{\partial}{\partial y}\left[\left[\frac{\overline{Q}_n(y,t)}{\delta} + \frac{1}{\beta}\right]\frac{\partial \overline{Q}_n(y,t)}{\partial y}\right] - \frac{L^2}{\mu_n}\frac{\partial \overline{Q}_n(y,t)}{\partial t}.$$

By assuming the weighting function to be uniform over the channel, weighted residual method requires that,

$$\int_0^1 R\, dy = 0$$

i.e.

$$\int_0^1 \left\{\frac{\partial}{\partial y}\left[\left[\frac{\overline{Q}_n(y,t)}{\delta} + \frac{1}{\beta}\right]\frac{\partial \overline{Q}_n(y,t)}{\partial y}\right] - \frac{L^2}{\mu_n}\frac{\partial \overline{Q}_n(y,t)}{\partial t}\right\} dy = 0 \tag{2.19}$$

Substituting equation (2.18) into (2.19) results in

$$\frac{dB(t)}{dt} = -6\frac{\mu_n}{\delta L^2}\left[(\alpha-\beta)^2 + B(t)(\alpha+\beta+2\delta\phi_T)\right] + 3(\dot{\alpha}+\dot{\beta}) \quad (2.20)$$

$$= f(\alpha(t), \beta(t), B(t))$$

where $\phi_T \equiv 1/\beta$ and $\dot{\alpha}$, $\dot{\beta}$ are the time derivatives of $\alpha(t)$ and $\beta(t)$.

$B(t)$ in equation (2.20) can now be solved using numerical methods for ordinary differential equations provided that suitable initial and boundary conditions are given.

For the initial condition $B(0)$, note that prior to the starting of the transient, all derivative terms in (2.20) must be zero, thus

$$B(0) = -\frac{(\alpha-\beta)^2}{(\alpha+\beta+2\delta\phi_T)}. \quad (2.20a)$$

For the boundary condition, one can use the method described in Section 2.2 which requires solving an implicit equation by iterative procedure. This method, however, is time consuming particularly in the weak inversion operation region. In the following section, a simple and efficient procedure is presented which avoids the iterative procedure.

2.4 Boundary Conditions for the Compact Model

The conventional method of solving for the carrier densities at both ends of the channel is to iteratively find the surface pontential near the source and drain of the MOSFET. In this section, however, $Q_n(0,t)$ and

$Q_n(1,t)$ are solved by analytically summing the weak inversion and strong inversion charges to get the total charge density. The charge summing method is more suitable for CAD applications. One may formulate this procedure by the following three sections.

2.4.1 Strong Inversion Charge Density

In strong inversion, the surface potential can be written as

$$\phi_s(y,t) = 2\phi_B + V(y)$$

where $V(y)$ is the voltage at point y in the channel, and ϕ_B is defined as

$$\phi_B = \frac{kT}{q}\ln\left[\frac{N_A}{n_i}\right].$$

Therefore, at the source and drain boundaries, the surface potentials are

$$\phi_s(0,t) = 2\phi_B$$

and

$$\phi_s(1,t) = 2\phi_B + V_D(t).$$

Substitute these two equations into (2.9n), gives normalized charge densities of

$$\beta_s(t) = Q_n(0,t) = V_G(t) - V_{T\beta}(t) \tag{2.21a}$$

and

$$\alpha_s(t) = Q_n(1,t) = V_G(t) - V_{T\alpha}(t) \tag{2.21b}$$

where

$$V_{T\beta}(t) \equiv V_{FB} + 2\phi_B + \lambda\sqrt{2\phi_B - V_B(t) - 1/\beta} \tag{2.21c}$$

and

$$V_{T\alpha}(t) \equiv V_{FB} + 2\phi_B + V_D(t) + \lambda\sqrt{2\phi_B - V_{BD}(t) - 1/\beta}. \qquad (2.21d)$$

Equations (2.21a) and (2.21b) give the charge densities for the source and drain ends in the strong inversion region.

2.4.2 Weak Inversion Charge Density

When either end of the channel is in the weak inversion region, the charge density is calculated by considering a MOSFET biased in the subthreshold region. Since $Q_n(y,t)$ is very small, equation (2.6) can be simplified as

$$I(y,t) = -\frac{Z\mu_n}{\beta}\frac{\partial Q_n}{\partial y}.$$

Integrating with respect to y, one obtains

$$I_D = -\frac{Z\mu_n}{L\beta}\Big[Q_n(y=L) - Q_n(y=0)\Big].$$

Since the source end is biased more negatively than the drain end,

$$Q_n(y=0) \gg Q_n(y=L)$$

one obtains,

$$I_D = \frac{Z\mu_n}{L\beta}Q_n(y=0). \qquad (2.22)$$

The subthreshold current is known to be proportional to $e^{\chi\beta\phi_s}$ [7], where χ stands for the nonideality factor resulting from surface state charge [3]. From (2.22), the charge density is also proportional to $e^{\chi\beta\phi_s}$, hence the

normalized subthreshold charge density may be written as

$$Q'_n(y=0) \equiv N_{AS}\, e^{[\,\chi\beta(V_G - V_T)]}$$

where $Q'_n(y=0)$ stands for the charge density and N_{AS} stands for the charge density at the threshold voltage. Both $Q'_n(y=0)$ and N_{AS} are normalized by C_{OX}. The charge density can thus be expressed as

$$Q_n(y=0) \equiv N_{AS}\, e^{[\,\chi\beta(V_G - V_T)]}\; C_{ox}\,. \qquad (2.23a)$$

N_{AS} and χ can be found by fitting (2.22) to the transistor's I-V characteristics. For example, a typical transistor I-V curve is plotted in Fig. 6, (V_{G1}, I_{D1}) and (V_{G2}, I_{D2}) are any two points below the threshold voltage V_T. From equation (2.22) and (2.23a), N_{AS} and χ can be solved as

$$\chi = \frac{1}{\beta(V_{G1} - V_{G2})} ln(\, I_{D1} / I_{D2}\,) \qquad (2.23b)$$

and

$$N_{AS} = \frac{I_{D1}L\beta}{Z\mu_n C_{ox}} e^{\chi\beta(V_T - V_{G1})} = \frac{I_{D2}L\beta}{Z\mu_n C_{ox}} e^{\chi\beta(V_T - V_{G2})}\,. \qquad (2.23c)$$

Equation (2.23a) expresses the boundary charge density in the weak inversion region as

$$n_{s\beta}(t) = N_{AS}\, e^{\chi\beta(V_G(t) - V_{T\beta}(t))}$$

where N_{AS}, χ, $V_{T\beta}$ are given in (2.23b), (2.23c), and (2.21c) respectively. To suppress the exponential increase of the charge density above the threshold region, an upper limit of this weak inversion charge was proposed by

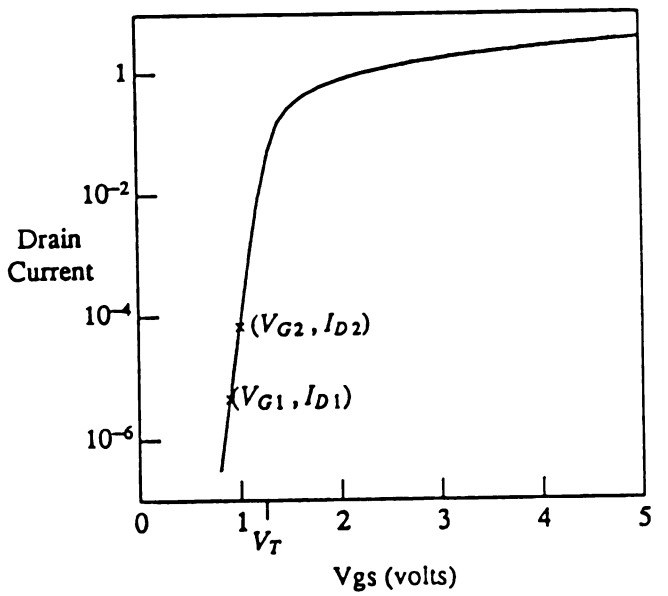

Fig. 6. Typical I-V characteristics for a MOSFET. The currents for gate voltages less than the threshold voltage exhibit exponential dependence on the gate voltage.

Antognetti and coworkers [5]. The upper limit was

$$n_x = \eta\, N_{AS}$$

where η is the suitable fitting parameter. The weak inversion charge density can be expressed by a continuous, smooth function given by

$$\beta_w(t) = \frac{n_{s\beta} n_x}{n_{s\beta} + n_x} \,. \tag{2.24a}$$

In a similiar manner, the boundary condition at the drain end can be derived as

$$\alpha_w(t) = \frac{n_{s\alpha} n_x}{n_{s\alpha} + n_x} \tag{2.24b}$$

where

$$n_{s\alpha} = N_{AS}\, e^{\chi\beta(V_G(t) - V_{T\alpha}(t))} \,.$$

2.4.3 Total Charge Density

For the transition between strong and weak inversion regions, the charge density in the strong inversion region and in the weak inversion region can be summed together to obtain the overall charge density as

$$\beta(t) = \beta_s + \beta_w \tag{2.25a}$$

and

$$\alpha(t) = \alpha_s + \alpha_w \tag{2.25b}$$

where β_s, β_w, α_s, α_w are give in equations (2.21) and (2.24) respectively. In Fig. 7, the strong inversion charge density, the weak inversion charge density, the charge density calculated from the conventional iterative

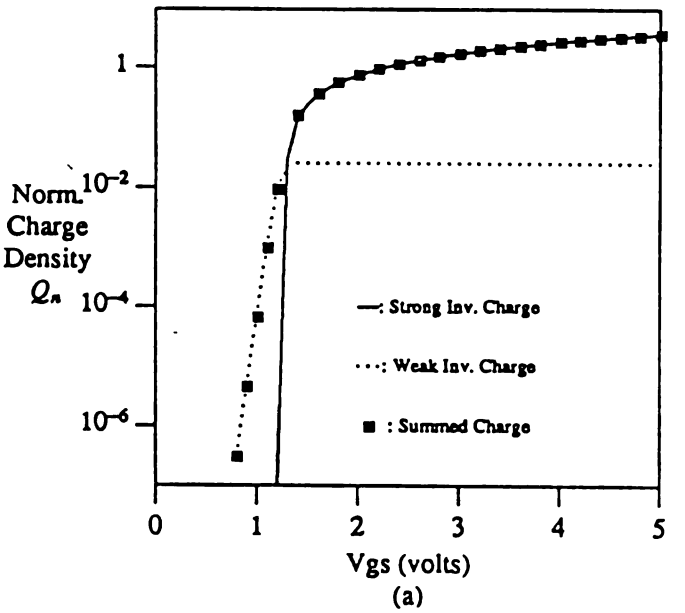

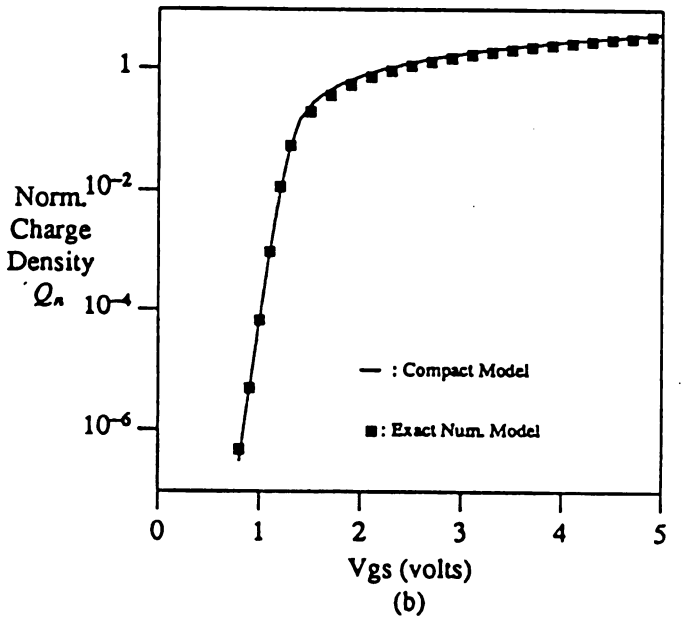

Fig. 7. (a) Illustration of the charge-summing method. The MOSFET parameters for the charge-summing method are: doping = 10^{15} cm^{-3}, flat band voltage = 0.3 volt, oxide thickness = 0.1 μm, N_{AS} = 0.1, χ = 0.7, η = 0.25. (b) Comparision between the I-V curves generated by the charge-summing and the exact numerical solution.

method and the charge density calculated from equation (2.25) are plotted to show the smoothness and accuracy of equation (2.25).

2.5 NQS Drain And Source Currents

The transient drain and source currents for the NQS model developed in Section 2.3 are derived in this section.

Integrating the normalized continuity equation (2.2n), one obtains

$$I(y,t) - I(0,t) = \frac{L^2}{\mu_n}\frac{d}{dt}\int_0^y Q_n(\zeta,t)\, d\zeta. \tag{2.26}$$

After one more integration, equation (2.26) becomes

$$\int_0^1 I(y,t)dy - I(0,t) = \frac{L^2}{\mu_n}\int_0^1\int_0^y Q_n(\zeta,t)d\zeta dy. \tag{2.27}$$

The integration on the right hand side of equation (2.27) can be simplified by integration-by-parts to be

$$\int_0^1\int_0^y Q_n(\zeta,t)d\zeta dy = \int_0^1 (1-y)Q_n(y,t)dy \tag{2.28}$$

Substituting equations (2.28), (2.10), (2.16) together, one obtains the expression for the source transient current to be

$$\begin{aligned} I_S(t) &= -I(0,t) \\ &= -\int_0^1\left[\frac{Q_n(y,t)}{\delta} + \frac{1}{\beta}\right]\frac{\partial Q_n(y,t)}{\partial y}dy + \frac{L^2}{\mu_n}\frac{d}{dt}\int_0^1(1-y)Q_n(y,t)dy. \end{aligned} \tag{2.29}$$

From (2.26) and (2.29), the expression for the transient drain current is

$$I_D(t) = I(1,t) = I(0,t) + \frac{L^2}{\mu_n}\frac{d}{dt}\int_0^y Q_n(\zeta,t)d\zeta$$

$$= \int_0^1 \left[\frac{Q_n(y,t)}{\delta} + \frac{1}{\beta}\right]\frac{\partial Q_n(y,t)}{\partial y}dy - \frac{L^2}{\mu_n}\frac{d}{dt}\int_0^1 yQ_n(y,t)dy. \quad (2.30)$$

The first term and second term of (2.29) and (2.30) may be identified as the dc current and transient current components respectively. By substituting the charge density Q_n given by (2.18) into (2.29), one obtains the expression of the transient source current of the compact model as

$$I_S(t) = \left[\frac{\alpha^2 - \beta^2}{2\delta} + \phi_T(\alpha - \beta)\right] - \frac{L^2}{\mu_n}\left[\frac{1}{6}\dot{\alpha} + \frac{1}{3}\dot{\beta} - \frac{1}{12}\dot{B}\right].$$

Substituting $\dot{B}$ of (2.20) into the above equation gives

$$I_S(t) = \left[\frac{\alpha^2 - \beta^2}{2\delta} + \phi_T(\alpha - \beta)\right]$$

$$- \frac{1}{2\delta}\left[(\alpha - \beta)^2 + B(\alpha + \beta + 2\delta\phi_T)\right] - \frac{1}{12}\frac{L^2}{\mu_n}(\dot{\beta} - \dot{\alpha}).$$

Noticing that the third term can be omitted to avoid the numerical complexity of calculating the difference between the derivatives [2], one obtains the final expression for source current to be

$$I_S(t) = \left[\frac{\alpha^2 - \beta^2}{2\delta} + \phi_T(\alpha - \beta)\right]$$

$$- \frac{1}{2\delta}\left[(\alpha - \beta)^2 + B(\alpha + \beta + 2\delta\phi_T)\right]. \quad (2.31)$$

The transient drain current can be similarly derived to be

$$I_D(t) = -\left[\frac{\alpha^2 - \beta^2}{2\delta} + \phi_T(\alpha - \beta)\right] - \frac{1}{2\delta}\left[(\alpha - \beta)^2 + B(\alpha + \beta + 2\delta\phi_T)\right] . \quad (2.32)$$

Since the first term and second term of (2.31) and (2.32) may be identified as the dc current and transient current components respectively [3]. (2.31) and (2.32) may be rewritten as

$$I_S(t) = -I_{DC}(t) - I_{TR}(t) \quad (2.33a)$$

$$I_D(t) = I_{DC}(t) - I_{TR}(t) , \quad (2.33b)$$

where I_{DC} and I_{TR} are defined as

$$I_{DC}(t) = \frac{\beta^2 - \alpha^2}{2\delta} + \phi_T(\beta - \alpha) \quad (2.33c)$$

and

$$I_{TR}(t) = \frac{1}{2\delta}\left[(\alpha - \beta)^2 + B(\alpha + \beta + 2\delta\phi_T)\right] . \quad (2.33d)$$

2.6 Further Improvements on the Compact Model

Comparisons were made between the compact model and the exact numerical model for the different operation regions. For example, the transient simulation described in Fig. 8 was performed on a MOSFET in the linear region. The transient currents of the compact model, the exact numerical model and the QS model are shown in Fig. 8(b). The charge distributions at several instants during the simulation are also shown in Fig. 8(c). It is seen that the compact model exhibits the non-quasi-static characteristics and that the quadratic approximation of the NQS charge

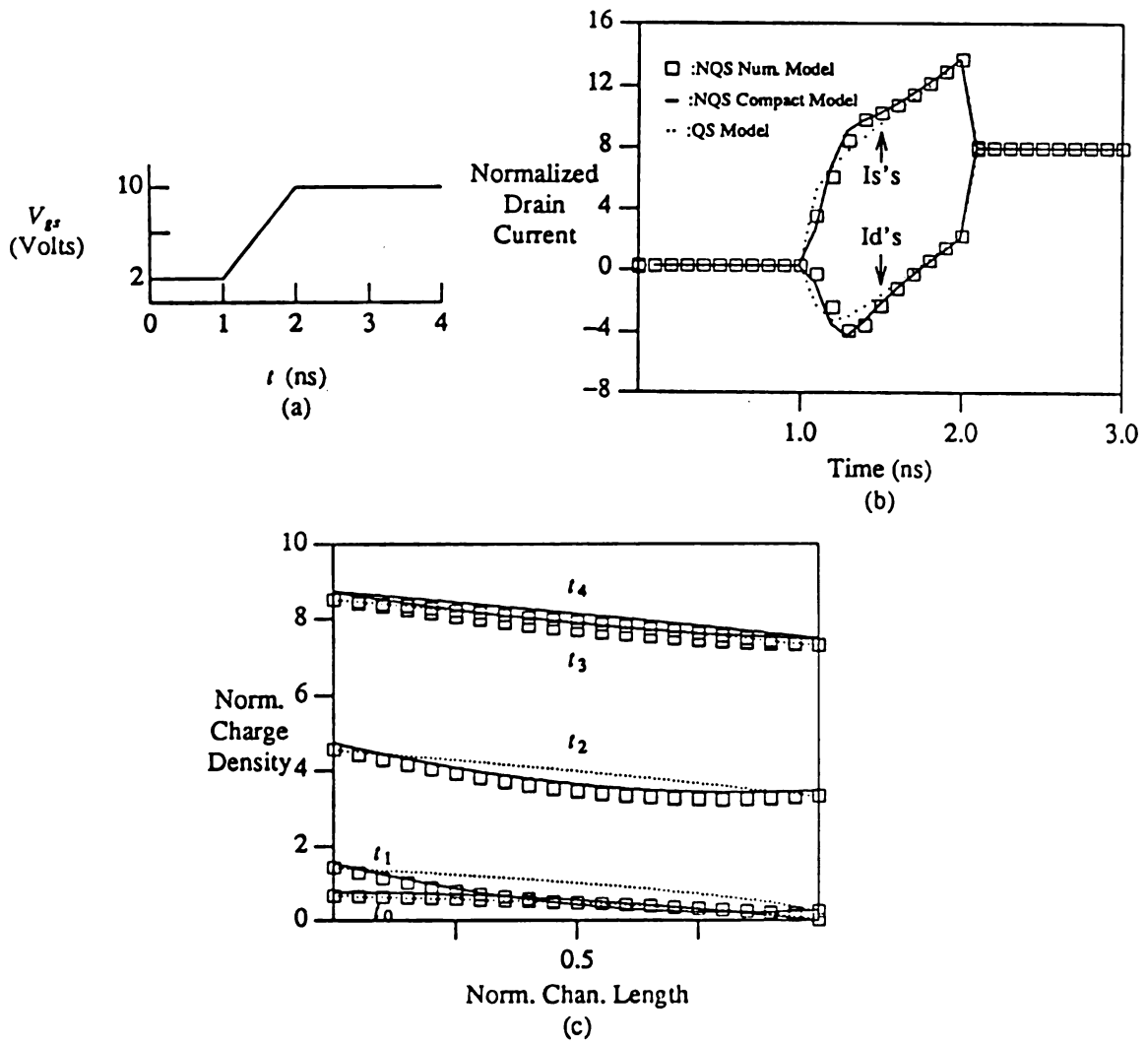

Fig. 8. Comparision between the NQS compact model, the NQS numerical solution and the QS model for a MOS-FET operating in the strong inversion region. (V_D = 1 volt, channel width = 10 μm, V_{FB} = 0.2 volt, doping = 10^{15} cm^{-3}, oxide thickness = 0.1 μm, V_{th} = 1.17 volt) (a) The voltage ramp applied to the gate is a (2-10) volt ramp in 1 ns. (b) Comparision between the transient drain and source currents generated by the above models. (c) Normalized charge density distributions at various times of simulation: t_0 = 1.0 ns, t_1 = 1.5 ns, t_3 = 2.0 ns, t_4 = 3.0 ns.

distribution (2.18) is in good agreement with the exact numerical model under strong inversion operation.

When the compact model is extended to the weak inversion operating region for fast operating speeds, it suffers some discrepancy that requires further changes to the model. To understand the discrepancy, consider the MOSFET operating as described in Fig. 9(a). The MOSFET is initially biased in the subthreshold region. A rising voltage ramp is then applied on the gate to turn the MOSFET from subthreshold to saturation region. From the charge distribution of the exact numerical model shown in Fig. 9(b), it is observed that the inversion charge injected from the source end needs some time to diffuse to the drain end. Therefore, a certain amount of delay time is expected before the transient drain current begins to increase as in Fig. 9(c).

Fig. 9(d) shows the simulation results of the compact model for the same operating conditions. The quadratic approximation of the charge distribution is inadequate in this situation since it predicts that the drain end is immediately affected after the ramp is applied. This inadequacy causes the erroneous jitter as shown in Fig. 9(e). The same discrepancy is observed for falling voltage ramps as shown in Fig. 10.

In order to overcome this inaccuracy, the following algorithm is

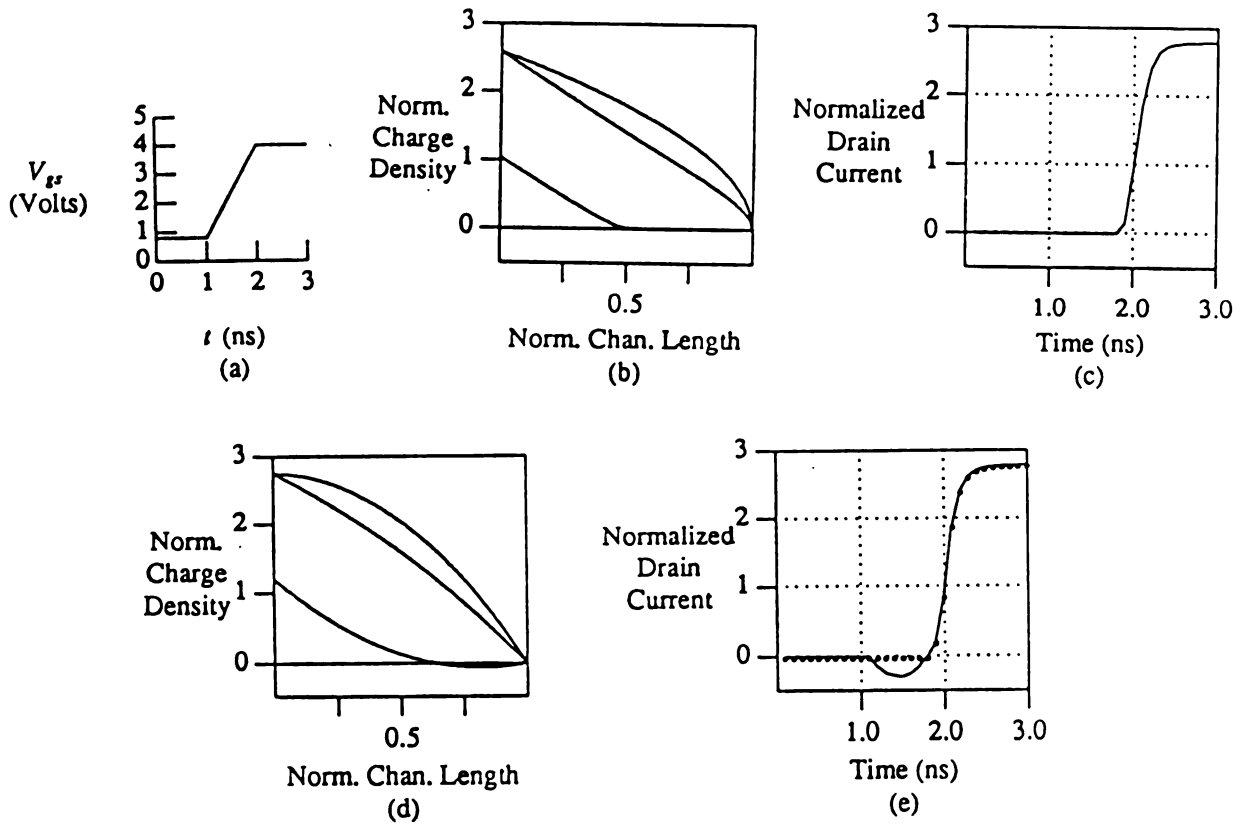

Fig. 9. Comparision between the NQS compact model and the NQS numerical solution for a MOSFET operating in weak inversion and saturation region. (V_D = 5 volt, the other physical quantities for the MOSFET's are the same as in Fig. 8) (a) The voltage ramp applied to the gate. (b) Numerical solution of the normalized charge density distributions at 1 ns, 1.5 ns, 2.0 ns and 3.0 ns. (c) The transient drain current generated by the NQS numerical solution. (d) The normalized charge density distribution generated by the quadratic approximation of the NQS compact model at time instants same as (c). (e) The current generated by the uncorrected compact model is represented by the solid line and the current generated by the correcting scheme is represented by the dotted curve.

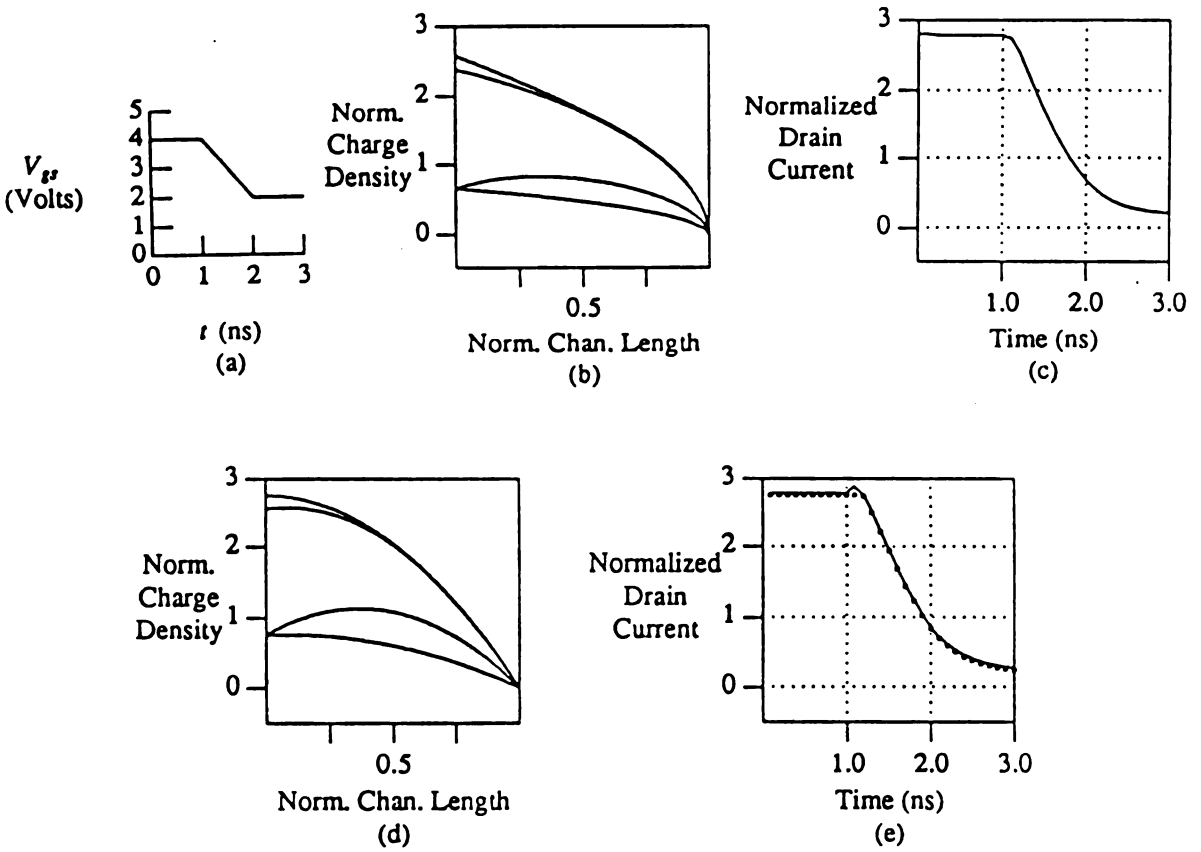

Fig. 10. Comparision between the NQS compact model and the NQS numerical solution for a MOSFET operating in saturation region. (V_D = 5 volt, the other physical quantities for the MOSFET's are the same as in Fig. 9.) (a) The voltage ramp applied to the gate. (b) Numerical solution of the normalized charge density distributions at 1 ns, 1.1 ns, 2.0 ns and 3.0 ns. (c) The transient drain current generated by the NQS numerical solution. (d) The normalized charge density distribution generated by the quadratic approximation of the NQS compact model at time instants same as (c). (e) The current generated by the uncorrected compact model is represented by the solid line and the current generated by the correcting scheme is represented by the dotted line.

implemented in the compact model:

1) IF (I_{DC} increasing) AND ($I_{TR} > 0$) AND (Drain end pinched-off),

   THEN:

      I_D is allowed to increase,

   ELSE,

      hold at it's previous value.

2) IF (I_{DC} decreasing) AND ($I_{TR} < 0$) AND (Drain end pinched-off),

   THEN:

      I_D is allowed to decrease,

   ELSE,

      hold at it's previous value.

This algorithm has been tested for all operation regions. The corrected I_D of this modified compact model is shown in Fig. 9(e) and Fig. 10(e) with the dotted line. It can be seen that not only the erroneous jitter is prevented but it also includes the delay for the conduction of the carriers from the source to the drain.

CHAPTER 3

Implementation of the Compact Device Model into Circuit Simulator

To investigate the significance of non-quasi-static effects in various MOSFET circuit applications, the NQS compact device model was implemented into a circuit simulator called TABLET (TABLE model based Transient simulator) [4]. MOSFET devices in the TABLET simulation program are represented by the model shown in Fig. 11. The MOSFET behavior is solved by evaluating the terminal charges and the drain to source dc current. The NQS effects are included in the four terminal charges: (1) $Q_D(t)$, the drain charge, (2) $Q_S(t)$, the source charge, (3) $Q_G(t)$, the gate charge and (4) $Q_B(t)$, the substrate charge. The formulation of the compact model for implementation in the TABLET simulation program expresses the four terminal charges in terms of the MOSFET device parameters (sizes, dopings, flat band voltage, gate oxide thickness, etc.) and the circuit parameters (biases on the terminals, time derivatives of the biases, etc.).

The expressions are developed in Section 3.1. The modifications to the original TABLET simulation program and the changes to the original user's manual are summarized in Section 3.2.

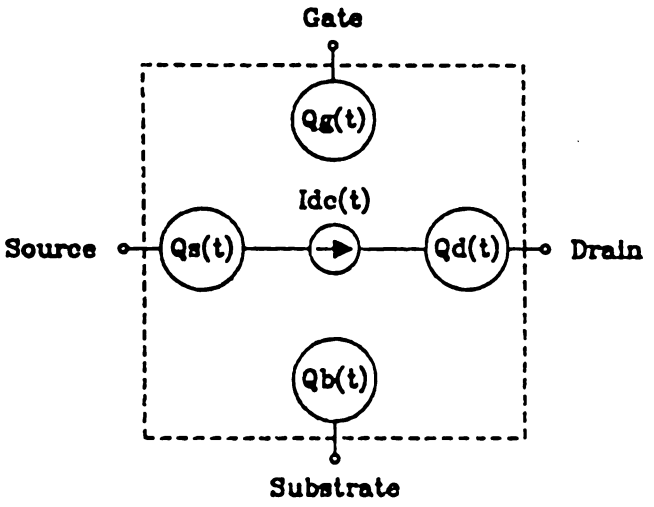

Fig. 11. Representation of the NQS compact model for the MOSFET device.

3.1 NQS Terminal Charges

In this section, the expressions for $Q_D(t)$, $Q_S(t)$, $Q_G(t)$, and $Q_B(t)$ are derived.

$Q_D(t)$ and $Q_S(t)$ are obtained by partitioning the total surface sheet charge, $Q_N(t) = \int_0^1 Q_n(y,t)dt$, according to the following definition [1,13]:

$$Q_D(t) = \int_0^1 yQ_n(y,t)dy \tag{3.1}$$

$$Q_S(t) = \int_0^1 (1-y)Q_n(y,t)dy\ . \tag{3.2}$$

By using (3.1) and (3.2), (2.29) and (2.30) can be written as

$$I_S(t) = -\ I_{DC}(t) + \frac{L^2}{\mu_n}\frac{d}{dt}Q_S(t) \tag{3.3}$$

and

$$I_D(t) = I_{DC}(t) - \frac{L^2}{\mu_n}\frac{d}{dt}Q_D(t). \tag{3.4}$$

By integrating (3.3) and (3.4), the source and drain terminal charges may be expressed as

$$Q_S(t) = Q_S(0) + \frac{\mu_n}{L^2}\int_0^t (\ I_S(t) + I_{DC}(t)\ )dt \tag{3.5}$$

and

$$Q_D(t) = Q_D(0) + \frac{\mu_n}{L^2}\int_0^t (\ I_{DC}(t) - I_D(t)\ )dt\ . \tag{3.6}$$

where $Q_S(0)$, $Q_D(0)$ are the initial terminal charges and I_S, I_D, and I_{DC} have already been derived in Section 2.6.

The use of (3.5) and (3.6) requires that the initial terminal charges $Q_D(0)$ and $Q_S(0)$ be calculated. The initial charge distribution may be approximated by

$$\overline{Q}_n(0) = \alpha(0)y + \beta(0)(1-y) + B(0)(y^2 - y)$$

where $\alpha(0)$, $\beta(0)$, $B(0)$ are given by equations (2.25a), (2.25b) and (2.20) respectively. Substituting $\overline{Q}_n$ into (3.1) and (3.2), one obtains the initial charges on the source and drain terminals as

$$Q_S(0) = \frac{1}{6}\alpha(0) + \frac{1}{3}\beta(0) - \frac{1}{12}B(0) \tag{3.7}$$

and

$$Q_D(0) = \frac{1}{3}\alpha(0) + \frac{1}{6}\beta(0) - \frac{1}{12}B(0). \tag{3.8}$$

Equations (3.5) to (3.8) are used in the circuit simulator to represent the charges for the source and the drain.

The gate terminal charge may be obtain by normalizing (2.7) according to Table 2.1 and integrating $Q_g(y,t)$ over the channel, i.e.

$$\begin{aligned} Q_G(t) &= \int_0^1 Q_g(y,t)dt \\ &= \int_0^1 \Big[V_G(t) - V_{FB} - \phi_s(y,t) \Big] dy \end{aligned} \tag{3.9}$$

where $\phi_s(y,t)$ may be solved by substituting the approximate charge

distribution $\overline{Q}_n$ of (2.18) into (2.12) to obtain the surface potential distribution.

$Q_B(t)$ may be obtain by solving the charge neutrality equation, i.e.

$$Q_B(t) = - Q_G(t) + Q_N(t) \tag{3.10}$$

where $Q_G(t)$ is derived in (3.7), and $Q_N(t) = Q_S(t) + Q_D(t)$.

3.2 NQS Circuit Simulator Implementation

Implementation of the NQS TABLET simulation program involved replacing the original MOSFET device model by the NQS compact MOSFET model. This required a change in the input file which describes the circuit and control commands of the simulator. To keep consistency with other device models in the simulator, all units and formats remained unchanged. The new MOSFET parameter description for the NQS models is listed in Appendix A.1. The valid output quantities listed in Table B-1 of the original TABLET user's manual [4] also required modification for the NQS MOSFET device model. The output quantities are listed in Appendix A.2.

CHAPTER 4

NQS Compact Model Applications

In this chapter, the NQS compact model developed in Chapter 3 is investigated in three applications. Application 1 presents the measurements of the drain current characteristics of the weak inversion and the strong inversion regions of a MOSFET. Drain current characteristics generated by the charge-summing method are then compared to the measured data. In application 2, transient signals are applied to an experimental circuit and the outputs are recorded. QS and NQS transient analysis are then performed to compare with the measurements. Comparision between the QS and the NQS analysis are also made for a different capacitive loading of the example circuit. Application 3 compares the transient drain and source currents charteristics between the QS model and NQS model of a single transistor operating in the subthreshold and the saturation region.

4.1 Application 1: Accurate I-V Characteristics by the Charge-Summing Method

The charge-summing method is used to simulate the characteristics of a MOSFET. The parameter values for the charge-summing method were selected to obtain a best fit with the measured drain current characteristics of a MOSFET.

The measurement setup for this application is shown in Fig. 12. The MOSFET was placed on the probe station with its terminals probed through the pads on the chip. The probes were then connected to the Semiconductor Parameter Analyzer HP 4145B which was programmed to connect a voltage source to the gate and a voltage source with current-metering to the drain. The source and substrate were connected to ground.

The drain current characteristics of a 100 μm × 100 μm transistor with $N_A = 2.34 \times 10^{16}\ cm^{-3}$ and T_{ox} = 0.0416 μm are shown in Fig. 13. The gate voltage varies from 0 to 5 volts and V_D = 1 and 5 volts respectively. The drain current characteristics calculated by the charge-summing method are represented by the solid line in Fig. 13 and the measurements are represents by the boxes.

The simulation results by the charge-summing method are in good agreement with the measurements on the weak and strong inversion current for this application.

4.2 Application 2: Transient Analysis of Resistor-MOS Transistor Circuit

In this example, a transient signal is applied to the input of the circuit shown in Fig. 15(a) where V_{DD} = 5 volts, R = 100 Ω and C_L = 100 pF. The loading capacitance was due to the parasitics of the chip and measure-

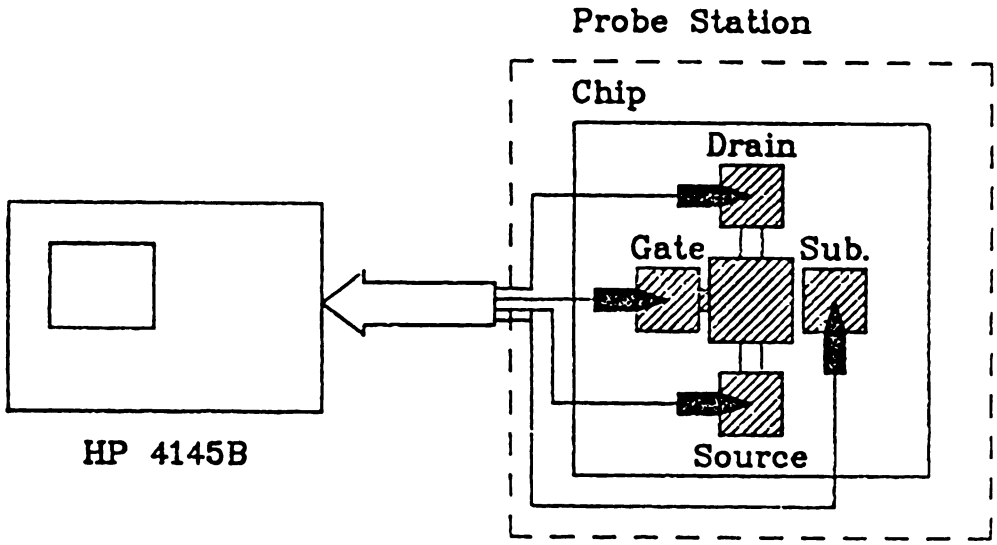

Fig. 12. Schematic diagram of the measurement setup for the application 1.

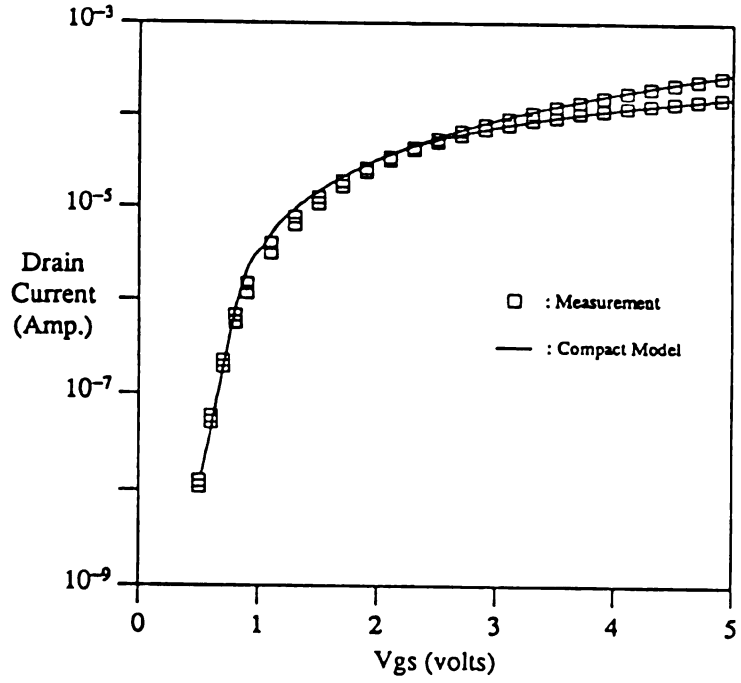

Fig. 13. I-V characteristics comparision. The parameters for the charge-summing method are :NAS = 5.2, KAI = 0.31, VFB = -0.6, MOB = 600, DEL = 1.8, ETA = 0.10.

ment equipments. The loading capacitance value was estimated by comparing simulated and measured results. The input voltage V_{IN} goes from 0 to 5 volts in 100 nanoseconds. The MOSFET used is the same as that described in Application 1.

The measurement setup for this application is shown in Fig. 14. The MOSFET is placed on the probe station with the source and substrate grounded. The Pulse/Function Generator HP 8116A and the Digitizing Oscilloscope HP 54200A are probed to the gate and the drain of the MOSFET respectively. A 100 Ω resistor is connected between the 5 volts power supply and the drain of the MOSFET. A 100 pF loading capacitor is also connected to the drain of the MOSFET.

The measurements, the analysis by the NQS compact model and the analysis by the QS model are represented by the squares, the solid line and the triangles in Fig. 15(b) respectively. A certain amount of time delay is required for the electrons to travel to the drain end before the drain current can begin to flow. This time delay of 100 ns is recorded for both the measurement and NQS simulation results. The QS model predictes an erroneous jitter for the output voltage due to the incorrect transient drain current shown in Fig. 15(c). A faster falling time of the output voltage might also be predicted by the QS model since the QS model assumes that

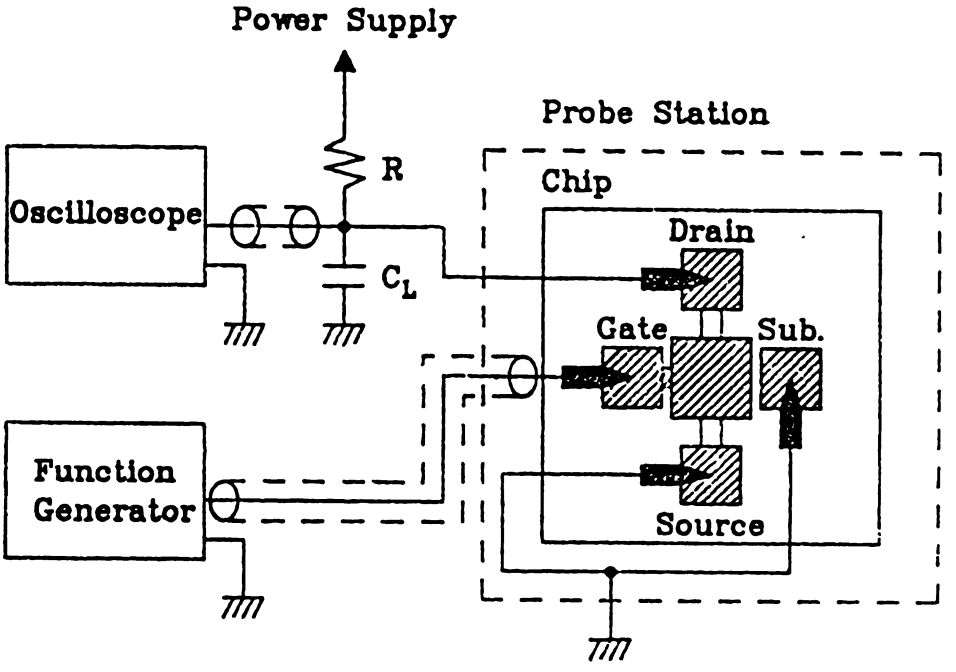

Fig. 14. Schematic diagram of the measurement setup for the application 2.

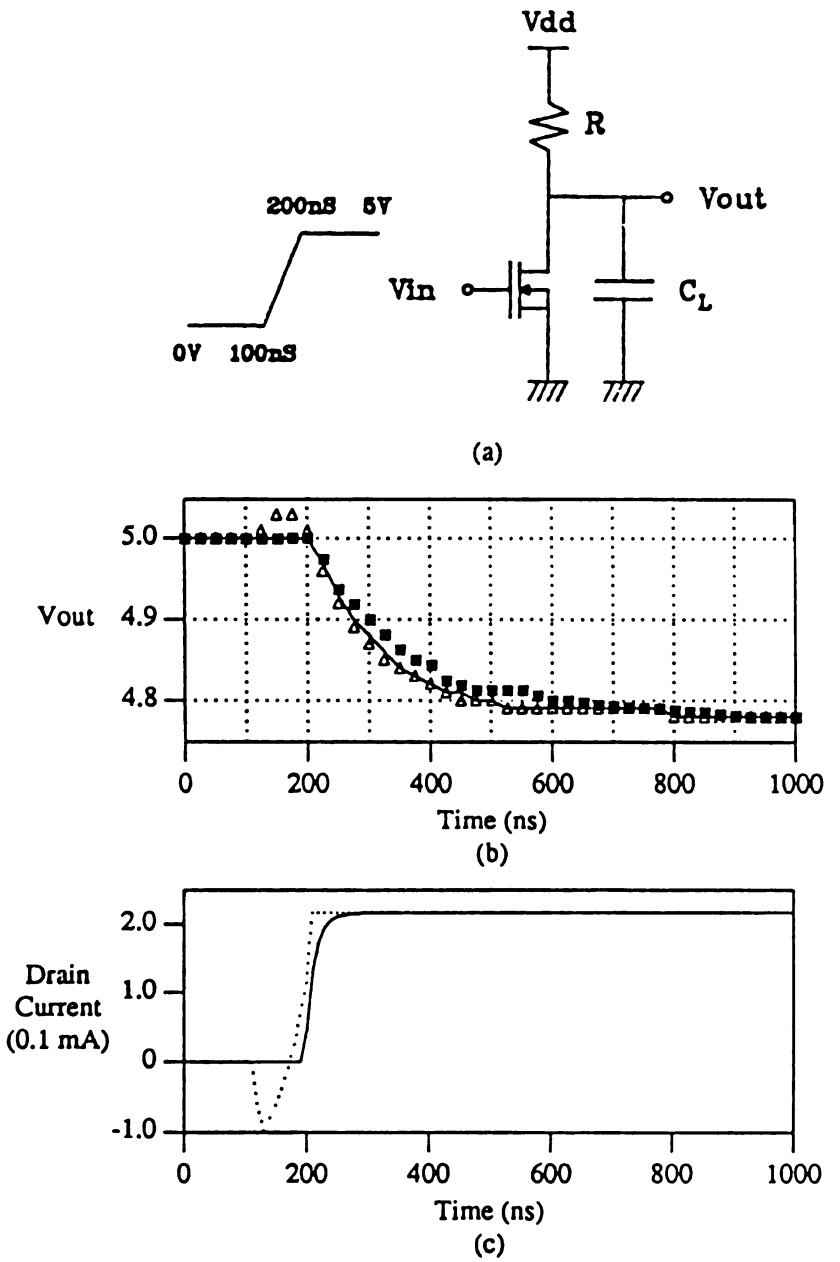

Fig. 15. Comparision between the measurements, NQS compact model and QS model. (a) The circuit used for this measurement. (b) Transient output voltage comparision: the squares are the measurements, the triangles are the QS results and the solid line is the result generated by the NQS TABLET simulator. (c) Transient drain currents by the NQS TABLET simulator (solid line) and the QS results (dotted line).

no delay time is required for the MOSFET to build up the channel charge. This instantaneous charge change causes a drain current to be present immediately. The drain current which discharges the capacitor thus causes the output voltage to change more rapidly for the QS model. For this experimental circuit, however, the load capacitor was large enough such that the time delays predicted by the NQS and QS simulations were in approximate agreement. To investigate the NQS model further, the simulation was repeated with a smaller capacitive load.

For a smaller capacitive load, the erroneous prediction of the jitter and the falling time by the QS model becomes more significant since the voltage change on a smaller capacitor is more pronounced for the same discharging currents. Fig. 16 shows this effect by using C_L = 10 pF.

4.3 Application 3: Transient Simulation in the Subthreshold Region

For a MOSFET operating in the region below threshold, the current transport mechanism is primarily due to the diffusion of the carriers. Thus, it requires a long time for the channel charge to be built up by the subthreshold current flows once the gate voltage varies. The QS model, which assumes that the channel charge distribution can be set up without time delay, predicts instantaneous current flows on both the source and drain end. Such erroneous predictions are less severe when the MOSFET

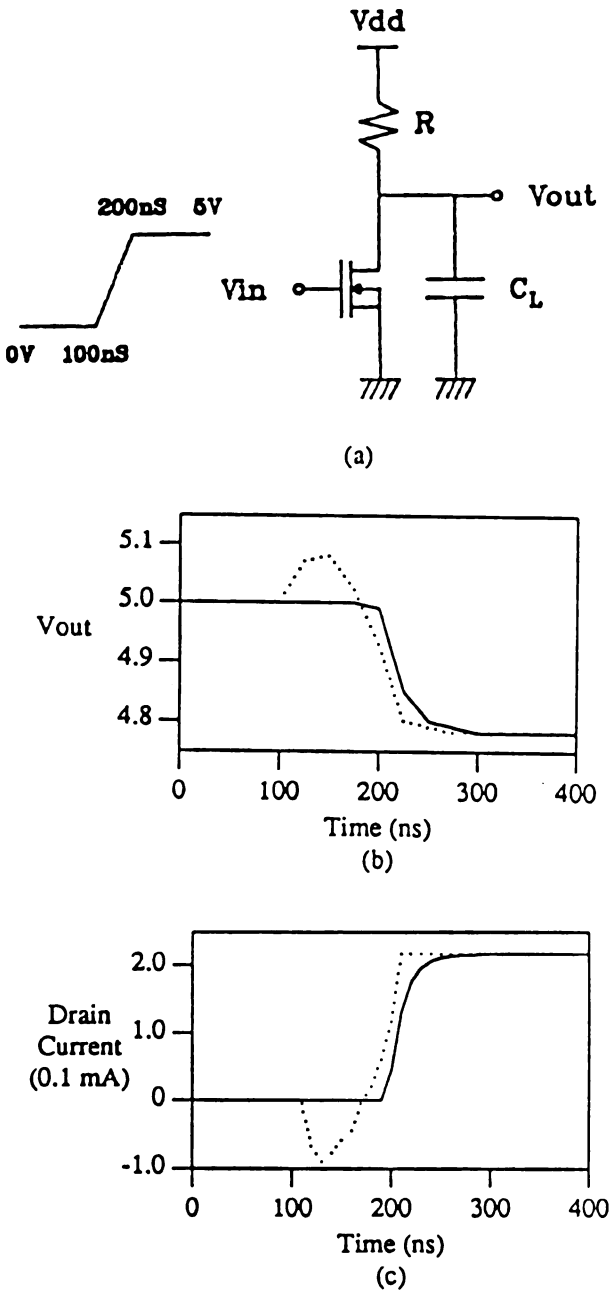

Fig. 16. Comparision between the NQS compact model and QS model for a smaller capacitive load. (a) The circuit used by this simulation. (b) Transient output voltage comparision: dotted line is the QS results and the solid line is the NQS TABLET simulator results. (c) Transient drain currents by the NQS TABLET simulator (solid line) and the QS model (dotted line).

is operating in the strong inverson region where the channel charge distribution can be set up by the faster drift current.

Fig. 17(b) and Fig. 17(c) show such effects when a 0.3 volt voltage ramp is applied to the gate of a 10 μm × 10 μm MOSFET. Fig. 17(b) compares the drain and source transient current for the NQS and QS simulations when a gate voltage ramp of 0.6 - 0.9 volt is applied to the MOSFET in the subthreshold region. Fig. 17(c) compares the drain and source transient current for the NQS and QS simulations when the same 0.3 V voltage ramp is applied in the saturation region.

It can be seen that the NQS and QS simulations show minimal difference for the MOSFET operating in the strong inversion region. In the weak inversion region, however, simulations with the QS assumption show erroneous negative drain currents when turning on the channel. Also, an incorrect rise time is predicted with the QS assumption.

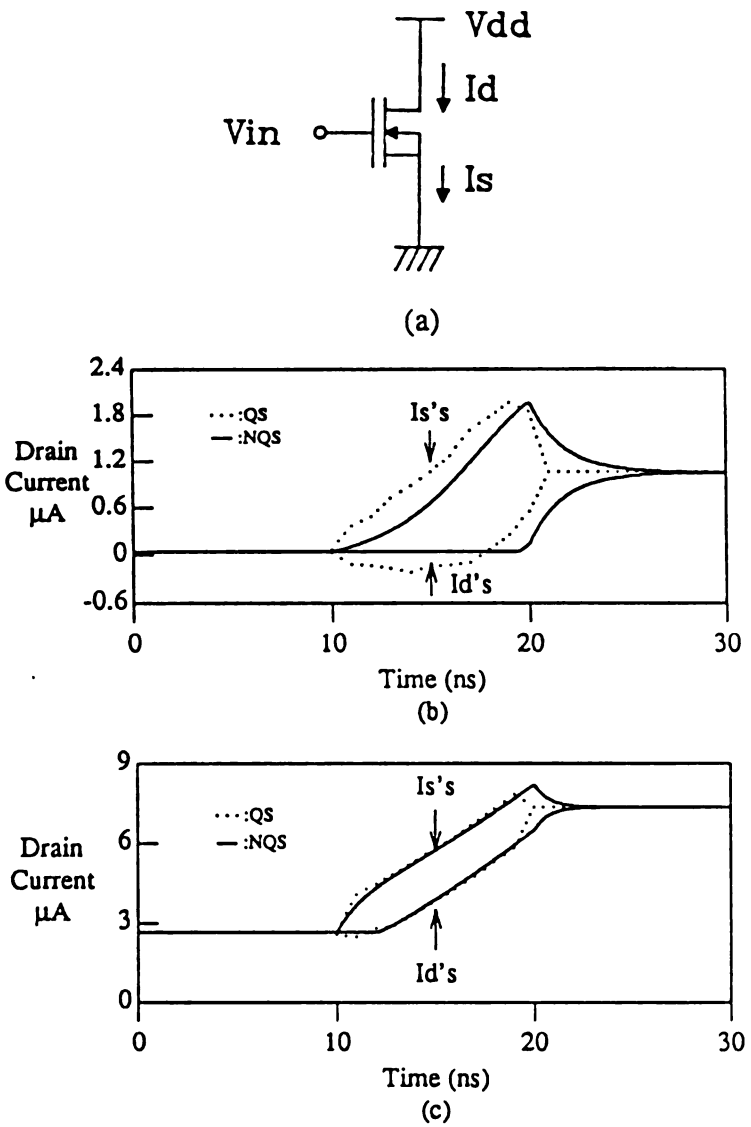

Fig. 17. Comparision between the NQS compact model and QS model under the weak inversion and strong inversion operating condition. (a) The circuit used by this simulation. The size of the MOSFET is 10 μm by 10 μm and the other physical quantities are the same as Fig. 14. (b) Subthreshold transient drain and source current characteristics by the NQS TABLET simulator (solid line) and the QS results (dotted line) when the gate voltage ramp is (0.6-0.9) volt in (10-20) ns. (c) Strong inversion transient drain and source current characteristics by the NQS TABLET simulator (solid line) and the QS results (dotted line) when the gate voltage ramp is (1.1-1.4) volt in (10-20) ns.

CHAPTER 5

Conclusions

A MOSFET device model which incorporates the NQS effect has been developed. This model accurately and efficiently predicts the MOSFET behavior in all regions of operation. In particular, the weak inversion region is included. This device model approximates the NQS charge distribution by a quadratic function which greatly reduces the computational time and thereby makes possible efficient NQS transient simulation. The use of the quadratic approximation for representing the spatial variation of the channel charge in the various regions of operation was studied and improvements were implemented for the subthreshold and saturation regions of operation.

The compact model results are in good agreement with the DC and the transient measurements described in Chapter 4. It is shown that the compact model predicts smooth and accurate DC characteristics both in the weak and strong inversion region. Comparision between the transient NQS and QS simulations showed that the NQS effects should be included for the accurate determination of circuit timing characteristics for falling or rising signals. In particular, circuits with small capacitive loadings are more susceptible to NQS charging or discharging currents. For circuits

with MOSFET's operating in the near-threshold or subthreshold region, the NQS effect should also be included due to the slower diffusion mechanism dominant in the moderate inversion region.

Appendix A - Changes to the TABLET User's Manual

A.1 - MOSFET Parameter Entries

The entries of the parameters for the MOSFET model of the NQS TABLET are listed and explained in the following:

CHAN Channel type (P or N)

DOP Substrate doping
symbol: N_A
units : $1/cm^3$

NAS Normalized charge density at the threshold voltage with the source and substrate grounded
symbol: N_{AS}
units : $1/F \cdot cm^3$

KAI Nonideality factor for the subthreshold current
symbol: χ
units : dimensionless

VFB Flat band voltage
symbol: V_{FB}
units : *volts*

MOB Mobility of the mobile charge
symbol: μ_n
units : cm^2 / *V–sec*

TOX Gate oxide thickness
symbol: t_{ox}
units : μm

DEL Short channel effect factor
symbol: δ
units : dimensionless

ETA Fitting parameter for the
weak inversion charge density
symbol : η
unit : dimensionless

A.2 Valid Output List for the MOSFET

The valid output for the MOSFET model of the NQS TABLET are listed in Table A.2.1. All quantities have units consistent with the TABLET program except for α, β, I_D, I_S which are normalized by Table 2.1.

Table A.2.1

Element Name	Var Value	Quantity	Unit
M	4	I_{DC}	mA
	5	C_{SB}	pF
	6	C_{DB}	pF
	7	C_{GS}	pF
	8	C_{GD}	pF
	9	C_{GB}	pF
	20	B	none
	21	α	V/cm^2
	23	β	V/cm^2
	29	Q_S	10^{-12} ·Coul.
	30	Q_D	10^{-12} ·Coul.
	31	Q_G	10^{-12} ·Coul.
	32	Q_B	10^{-12} ·Coul.
	34	I_D	V^2
	40	I_S	V^2

List of Reference

1. P. Yang and P. K. Chatterjee, "Spice Modeling for Small Geometry MOSFET Circuits," *IEEE Tran. Computer-Aided Des.*, vol. CAD-1, pp. 169-182, 1982.

2. P. Mancini, C. Turchetti, and G. Masetti, "A Non-Quasi-Static Analysis of the Transient Behavior of the Long-Channel MOST Valid in All Regions of Operation," *IEEE Tran. on Electron Devices,* vol. ED-34, no. 2, pp. 325-334, February 1987.

3. C. Turchetti, P. Mancini, and G. Masetti, "A CAD-Oriented Non-Quasi-Static Approach for the Transient Analysis of MOS IC's," *IEEE Journal of Solid-State Circuits,* vol. SC-21, pp. 827-835, October 1986.

4. T. Grotjohn, *Investigation of Unified Table and Analytic Models for Accurate Circuit Simulator,* TR-EE 86-37, Purdue University, December 1986.

5. P. Antognetti, D. D. Caviglia, and E. Profumo, "CAD Model for Threshold and Subthreshold Conduction in MOSFET's," *IEEE Journal of Solid-State Circuits,* vol. SC-17, no. 3, pp. 454-458, June 1982.

6. H. C. Pao and C. T. Sah, "Effects of Diffusion Current on Characteristics of Metal-Oxide(Insulator)-Semiconductor Transistors," *Solid-State Electronics,* vol. 9, pp. 927-937, 1966.

7. J. R. Brews, "A Charge-Sheet Model of the MOSFET," *Solid-State Electronics,* vol. 21, pp. 345-355, 1978.

8. C. Turchetti, "Relationships for the Drift and the Diffusion Components of the Drain Current in a MOS Transistor," *Electron Letter,* vol. 19, pp. 960-962, 1983.

9. S. M. Sze, *Physics of the Semiconductor Devices (Second Edition),* John Wiley and Sons, New York, 1981.

10. S. Liu and L. W. Nagel, "Small Signal MOSFET Models for Analog Circuit Design," *IEEE Journal of Solid-State Circuits,* vol. SC-17, pp. 983-998, 1982.

11. M. Bagheri and Y. Tsividis, "A Small Signal dc-to-High-Frequency Nonquasistatic Model for the Four-Terminal MOSFET Valid in All Regions of Operations," *IEEE Tran. on Electron Devices,* vol. ED-32, no. 11, November 1985.

12. G. Merckel, J. Borel, and N. Z. Cupcea, "An accurate Large-Signal MOS Transistor Model for Use in Computer-Aided Design," *IEEE Tran. on Electron Devices,* vol. ED-19, no. 5, pp. 681-690, May 1972.

13. S. Y. Oh, D. E. Ward, and R. W. Dutton, "Transient Analysis of MOS Transistor," *IEEE Tran. on Electron Devices,* vol. ED-27, pp. 1571-1578, 1980.